analytical chemistry

Article

Cite This: Anal. Chem. 2018, 90, 9040−9047

pubs.acs.org/ac

A Transferable, Sample-Independent Calibration Procedure for Trapped Ion Mobility Spectrometry (TIMS)

Mengqi Chai,[†] Meggie N. Young,[†] Fanny C. Liu,[†] and Christian Bleiholder*[,†,‡]

[†]Department of Chemistry and Biochemistry and [‡]Institute of Molecular Biophysics, Florida State University, Tallahassee, Florida 32306-4390, United States

Supporting Information

ABSTRACT: Ion mobility spectrometry-mass spectrometry (IMS-MS) determines momentum transfer cross sections of ions to elucidate their structures. Recent IMS methods employ electrodynamic fields or nonstationary buffer gases to separate ions. These methods require a calibration procedure to determine ion mobilities from the experimental data. This applies in particular to trapped IMS (TIMS), a novel IMS method with reported high resolving powers. Here, we report the first systematic assessment of the accuracy and the limitations of mobility calibration in TIMS. Our data show that the currently used TIMS calibration approach reproduces drift tube mobilities to approximately 1% (95th percentile). Furthermore, we develop a transferable and sample-independent calibration procedure for TIMS. The central aspects of our approach are (1) a calibration function derived from a solution to the Boltzmann transport equation and (2) calibration constants based on a Taylor expansion of instrument properties (TEIP). The key advantage of our calibration approach over current ones is its transferability: one equation and one set of parameters are sufficient to calibrate ion mobilities for various instrument settings, compound classes, or charge states. Our approach is transferable over time and sufficiently accurate (~1−2%) for structure-elucidation purposes. While we develop our calibration procedure specifically for TIMS, the approach we take is generic in nature and can be applied to other IMS systems.

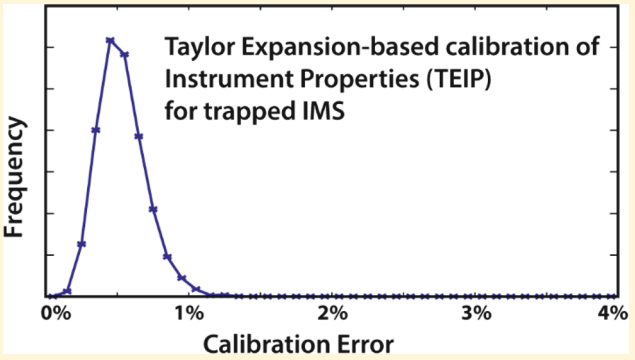

Ion mobility spectrometry-mass spectrometry (IMS-MS) separates ions by their mobility K and m/z ratio.[1−3] The ion mobility K can be converted into a momentum transfer cross section Ω to characterize the ion structure via[1,2]

$$K_0 = \frac{3q}{16N_0}\sqrt{\frac{2\pi}{\mu k_B T}}\cdot\frac{1}{\Omega} \quad (1)$$

In this equation, q is the charge of the analyte ion; T and N_0 are the temperature and reduced number density of the buffer gas; k_B is the Boltzmann constant; μ is the reduced mass of the ion-neutral pair; and K_0 is the reduced ion mobility, which is trivially related to K.[2]

The accuracy of the measured cross sections takes on increased significance in a range of applications. For example, cross sections enable IMS-MS to elucidate structures of complex and dynamic biological systems,[4−6] including amyloid assemblies,[7−9] viral capsids,[10] and other biological complexes.[11−13] Cross sections and ion mobilities are also used to characterize[14−18] and select[19] small peptides in metabolomics or proteomics studies that couple IMS-MS to liquid chromatography (LC).

Conceptually, measuring ion cross sections in IMS is simple: an electric field forces ions to move through a diluted buffer gas.[1−3,20] For a given charge, ions with small cross sections experience less friction from collisions with buffer gas particles and, thus, travel faster than ions with large cross sections. Hence, by measuring the time t_m it takes an ion to traverse a given distance in the buffer gas, one can obtain its mobility. However, various types of IMS-MS differ in their ability to measure ion mobilities.[3]

For drift tube ion mobility instruments, which use stationary buffer gases and static, uniform electric fields, the ion physics are well-known.[3,16,21−23] The mobility of an ion can thus be directly obtained from the measured arrival times. The ion physics, however, are less understood for instruments that separate ions by electrodynamic fields or nonstationary buffer gases.[20] These instruments include the commercially available traveling-wave[24] and trapped[20,25−27] IMS systems and also structures for lossless ion manipulations (SLIM) using traveling-waves.[28] These instruments currently require a calibration procedure to convert t_m into K_0.

In principle, ion mobility calibration is not overtly complicated; one requires (1) a calibration function and (2) calibrants. Nevertheless, and despite significant efforts,[11,15,29] an accurate calibration procedure that is robust for different compound classes, charge states, or different instrument

Received: March 23, 2018
Accepted: July 5, 2018
Published: July 5, 2018

DOI: 10.1021/acs.analchem.8b01326
Anal. Chem. 2018, 90, 9040−9047

settings is unknown. Our objective here is to develop such a calibration procedure for trapped IMS (TIMS), but the approach we take is generic in nature and can be applied to other IMS systems.

The empirical calibration function used in trapped IMS (TIMS) is[30,31]

$$K_0 = a + \frac{b}{V_m} \quad (2)$$

where a and b are calibration constants and V_m is approximately the voltage across the TIMS analyzer when the ion is measured. Equation 2 has been successfully used to calibrate TIMS spectra. For example, cross sections calibrated for ubiquitin[5,32] or cytochrome c[33] agree well with the corresponding drift tube values. More recently, we constructed a tandem-TIMS device by coupling two TIMS analyzers and calibrated tandem-TIMS spectra according to eq 2.[34] Cross sections calibrated for ubiquitin spectra obtained by tandem-TIMS also closely match the corresponding drift tube values reported by Bleiholder et al.[35] Nevertheless, the constants a and b depend highly, and in an unknown manner, on the TIMS operating settings. This is a consequence of the empirical nature of the calibration function and a significant drawback because any change in the TIMS settings requires a recalibration. This situation is encountered, for example, when the operator changes settings to "zoom" into a narrow mobility range for high resolving power. A key aspect of our work here is to devise calibration coefficients that are, to a good approximation, truly constant and independent of instrument settings or sample properties.

Perfluoro-phosphazenes contained in Agilent ESI tune mix are typically used as calibrants for TIMS.[30,31] In a recent contribution to this journal,[36] Haler et al. argue that TIMS mobilities are more accurate when sodiated polyethylene glycol (PEG, also called poly(ethylene oxide)/PEO) is used as calibrants (∼1%) as opposed to Agilent tune mix (∼5%).[36] These results are significant because errors about 5% would largely invalidate previous work with TIMS.[5,17,31−34,37]

The conclusions made by Haler et al. that PEG is a superior ion mobility calibrant than perfluoro-phosphazenes, however, must be reconsidered in light of the following.

First, Haler et al.[36] base their conclusions on a single setting for TIMS operation. It is, however, unclear if their findings can be extrapolated to measurements made under different operating conditions. Second, Haler et al.[36] calibrate with tune mix ion mobilities that were reported[30] to be themselves calibrated from TIMS spectra but not measured on a drift tube.[38] By contrast, their PEG reference mobilities are measured on a drift tube. The observed inferior performance of the phosphazenes could thus be rationalized by inaccurate calibrant mobilities. Finally, Haler et al.[36] refer to work published by Wyttenbach et al. and von Helden et al.[39,40] to assert that "single-cation adducts such as sodium adducts of PEO [PEG] have an easily predictable shape (spherical shape) which was additionally established to be temperature-independent" and that "PEO [PEG] polymer−cation complexes have robust shapes and do not exhibit any change in conformations or any appearance of new stable shapes upon ion heating.". In the referenced papers, however, the authors state the exact opposite, namely, that "[structures of sodiated] PEG systems start to oscillate significantly for T > 300 K, as their internal temperature increases, with the net effect that their average "size" or cross sections will increase" and that "the bigger the system gets, the more it "expands" with temperature" as "a consequence of the fact that only seven or eight of the oxygen atoms can coordinate with [sic] Na+ ion".[40] More recently,[41] Wyttenbach et al. point out that "[c]harge-remote loops and ends of the polymer chain break away from and return back to the surface of the ion-neutral cluster. This motion increases in frequency and amplitude as the temperature rises".[41] It appears, therefore, likely that PEG ions change their structures, and thus their mobilities, as they gain internal energy from electric fields in IMS measurements.[32,42] Since different instruments heat ions to different internal temperatures,[16,27,43,44] PEG ions, thus, likely take on different structures in the drift tube reference measurements than when calibrating TIMS or traveling wave instruments. These observations for PEG are contrasted by temperature-dependent data recorded by Ujma et al. for the m/z 622, 922, and 1222 phosphazenes,[23] which reveal that their cross sections decrease monotonically with temperature as expected for a given structure.

These discussions demonstrate the significance for a more generic calibration method, capable of accurately calibrating ion mobilities for different classes of compounds, charge states, or operating settings. Here, we describe such a generic calibration procedure for trapped IMS (TIMS). Our calibration strategy differs from previous approaches in three key aspects. First, our calibration function is based on a solution to the Boltzmann transport equation but is not motivated by empirical observations. Second, we separate quantities that depend on the sample from those that depend on the instrument. Third, we perform a Taylor expansion for the instrument-dependent quantities and calibrate the Taylor expansion coefficients. The result is an accurate, robust, and transferable calibration procedure for a trapped IMS instrument. The overall strategy is generic, however, and can be applied to other IMS systems as well.

EXPERIMENTAL DETAILS

Materials and Sample Preparation. Agilent ESI tuning mix solution (G2421A) was used as obtained. Solvents were LC/MS grade water, methanol, isopropanol, and acetonitrile. Tetraalkylammonium (TAA) salts with varying alkyl chain lengths were prepared as described[16] and were combined to a final concentration of ∼1 μg/mL of each salt. A 10 μg/mL mixture of the pentapeptides SDGRG and GRGDS (Sigma-Aldrich) was prepared in 50:50 (v:v) MeOH:H_2O. Ubiquitin solutions (100 μM) were prepared from bovine erythrocytes (≥98%, Sigma-Aldrich). More details are found in section S3 of the Supporting Information.

Trapped Ion Mobility Spectrometry. Samples were infused into the electrospray ionization (ESI) source in positive mode through a gastight syringe. Nitrogen was supplied from a nitrogen generator (Peak Scientific, NM32-LA-MS-230 V). The flow rate and temperature of the desolvation gas were set to 4 L/min and 50 °C, respectively. Measurements were carried out over the course of 11 months. Agilent ESI tune mix spectra were recorded at the beginning (TM1) and at the end of the 11-month period (TM2) for various TIMS settings. The nitrogen generator was serviced, and the pump controlling the pressure in TIMS was replaced during that time frame. Spectra for SDGRG/GRGDS were recorded before (PM1) and after this maintenance occurred (PM2; these settings are identical to those used to record

DOI: 10.1021/acs.analchem.8b01326
Anal. Chem. 2018, 90, 9040−9047

TM2). Spectra for aqueous ubiquitin solutions were recorded throughout the time frame. See Tables S7−S14 for more details.

Calibrants and Reference Mobilities. We calibrate with several phosphazenes contained in high concentration Agilent ESI tune mix. Ion mobilities for the tune mix compounds were calculated with eq 1 from the cross sections reported by Stow et al.[38] These values closely match those previously used by us[5,20,32,34] and others.[31,45] Section S1.1 of the Supporting Information compares tune mix mobilities from different sources.

RESULTS AND DISCUSSION

Empirical Calibration Models. TIMS separates ions in the analyzer (Figure 1), which is composed of 25 segmented

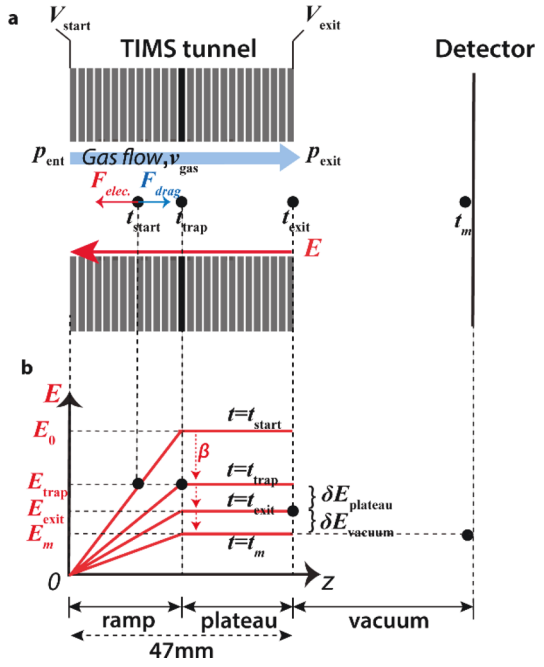

Figure 1. Schematics of the TIMS analyzer tunnel. (a) The pressure difference between the tunnel entrance and exit (p_{ent} and p_{exit}) induces a gas flow v_{gas} that drags ions to the exit ($\mathbf{F}_{drag}$, blue). The voltages applied to the first and last electrodes (V_{start} and V_{exit}) create a force on the ion ($\mathbf{F}_{elec}$, red) that opposes the drag force. (b) The electric field $\mathbf{E}$ increases in strength linearly with position in the first half of the analyzer tunnel (ramp) and remains constant in the second half (plateau). At time t_{start}, ions are trapped at an electric field strength E_{trap} with $\mathbf{F}_{drag} = -\mathbf{F}_{elec}$. As the electric field strength is reduced at rate β, ions move onto the plateau region at time t_{trap}, leave the TIMS analyzer at time t_{exit}, and reach the detector at time t_m. The electric field changes by $\delta E_{plateau}$ and δE_{vacuum}, respectively, while the ion traverses the plateau and vacuum regions.

ring electrodes with gaps sealed by spacers and o-rings. The operator regulates the pressures at the tunnel entrance and exit (p_{ent} and p_{exit}) to define a gas stream through the tunnel with velocity v_{gas}. The operator also controls the voltages on the first and last electrodes of the analyzer (V_{start} and V_{exit}), to create an electric field profile. The forces on the ions caused by the gas flow and electric field counteract each other: while the gas flow "drags" the ions toward the analyzer exit, the electric field pushes them back toward the entrance. As a result, ions are trapped on the "ramp" where the two forces cancel (Figure 1). Ions are eluted from the analyzer as the operator decreases the electric field strength at rate β. More details are given elsewhere.[20,25−27,30]

Ions traverse three regions before reaching the detector ("ramp", "plateau", "vacuum", Figure 1). Ions drift at velocity $v_{gas}=K\cdot E_{trap}$ in the ramp region while they do not drift in the other two regions.[20] Thus, ignoring the ion motion in the plateau and vacuum regions, one can approximate K_0 as[26,30]

$$K_0 = \frac{p}{p_0}\frac{T_0}{T}\frac{v_{gas}}{E_{trap}} \approx a + \frac{b}{V_m} \quad (3)$$

where the definition of the reduced mobility $K_0 = K\frac{p}{p_0}\frac{T_0}{T}$ was used; V_m is the voltage across the TIMS analyzer when the ion is detected at time t_m; T_0 and p_0 are the standard temperature (273.15 K) and pressure (1013.25 mbar). The right-hand side of eq 3 is identical to the current TIMS calibration function given in eq 2. Thus, eq 2 introduces a systematic error because it inaccurately reflects the time the ion spends on the plateau and vacuum regions (Figure 1). Details are given in section S1.3 of the Supporting Information.

We measure TIMS spectra for phosphazenes m/z 622, 922, 1522, and 2122 of high concentration ESI tune mix for various ramp rates β. We then calibrate mobilities according to eq 2 and assess their accuracy by leave-one-out cross validation (for details see Tables S4−S6). Figure 2a shows that the error of the calibrated mobilities (defined as deviation from the drift tube values reported by Stow et al.[38]) increases systematically with ramp rate β. This observation underscores the systematic error in eq 2: the current calibration approach works well at low values for β because here the time the ions spend on the ramp dominates over the time the ions spend on the plateau and vacuum regions. The data also show that the error becomes larger when the intercept a is excluded from the fit. This indicates that the intercept in eq 2 empirically accounts for the ion motion outside the ramp region.

Overall, Figure 2a shows that calibrating according to eq 2 reproduces drift tube mobilities to better than 2% for all ramp rates studied. Note that our calibrated mobilities are more accurate than what was reported by Haler et al.[36] for this calibration procedure, which we rationalize by more accurate calibrant mobilities in our work.

Next, we assess the performance for small peptides. To this end, we calibrate mobilities for the pentapeptides SDGRG and GRGDS at various ramp rates (β < 430 V/cm/s) and calculate the error as the deviation from drift tube mobilities taken from May et al. (for details see Table S7).[16] The resulting error distribution is plotted in Figure 2b. The data show that the current calibration approach accurately reproduces the corresponding drift tube mobilities: the 95th percentiles are 0.8% and 1.2% (see Table 1). Our results thus underscore the validity of the current calibration approach for operating conditions typically used with TIMS.[5,17,31−34,37] Our data, again, indicate a significantly higher accuracy than Haler et al.[36] who reported that calibrated mobilities for similar peptide systems deviate by up to ∼7% from the drift tube values.

Figure 2c and 2d correlate the slope b of the calibration function to the ramp rate β and entrance pressure p_{ent}, respectively. The plots show that b depends strongly on β as well as on p_{ent}. Equivalent observations are made in Figure S3 for the intercept a. The data thus demonstrate that the calibration coefficients a and b are not transferable to different measurement settings, such as different ramp rates or gas

DOI: 10.1021/acs.analchem.8b01326
Anal. Chem. 2018, 90, 9040−9047

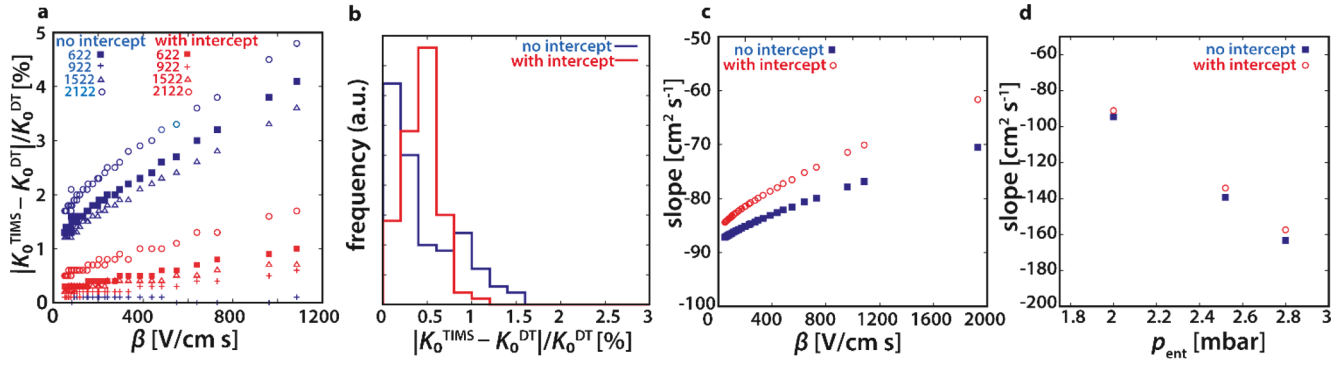

Figure 2. Performance of currently used TIMS calibration models. (a) Relative error of calibrated mobilities K_0^{TIMS} as a function of ramp rate β. The error increases with increasing ramp rate β. Errors are <2% if the intercept is included in the calibration. (b) Frequency distributions of the relative error of calibrated TIMS mobilities for the pentapeptides SDGRG and GRGDS measured at ramp rates β < 430 V/cm/s. The models achieve 95th percentiles of 0.8% (with intercept) and 1.2% (no intercept). (c, d) Correlations of the slope b of the currently used calibration function to the ramp rate β and entrance pressure p_{ent} show that b depends significantly on β and p_{ent}.

Table 1. Accuracy of Various Ccalibration Procedures for Protonated and Sodiated SDGRG and GRGDS[a,b,c]

	currently used calibration models[d]		TEIP (this work)	
	with intercept	without intercept	(2, 1, 1)	(4, 2, 1)
mean	0.4	0.5	0.8	0.5
67%-ile	0.5	0.5	1.0	0.7
95%-ile	0.8	1.2	1.7	1.0

[a]Drift tube values taken from May et al.[16] [b]Errors in percent deviation from the drift tube values. [c]TM2 was used for calibration. [d]Equation 2 was used as calibration function where a and b are fitted ("with intercept") or a is set to zero ("without intercept").

pressures. This lack of transferability of the calibration coefficients means that continued recalibration must be performed whenever the operator changes experimental settings.

A Transferable, Sample-Independent Calibration for TIMS. *Transferable and Sample-Independent Calibration Function.* Our first step in developing a transferable, sample-independent calibration function is to start with a solution to the Boltzmann transport equation for TIMS.[20] For sake of simplicity, we define $E_m \equiv E_0 - \beta t_m$ as the electric field strength on the plateau region at the time the ion is detected. This allows us to write the relationship between K_0 and E_m (Figure 1) as

$$E_m \equiv E_0 - t_m\theta^2 = \frac{g}{K_0} - \sqrt{\frac{l}{K_0}}\theta - t_0\theta^2 \tag{4}$$

where we define $\theta \overset{\text{def}}{=} \sqrt{\beta}$ and where E_0 is the initial electric field strength of the plateau. The term g corresponds to the effective drift velocity on the ramp and l to the effective length of the plateau (see sections S1.4 and S1.5 of the Supporting Information for more details). The last term, t_0, corresponds to the time an ion takes to traverse the vacuum region. What is important is this: since we know how eq 4 is derived from a solution to the Boltzmann transport equation,[20] we know that g and l depend on p_{ent} and also that they do not depend on sample properties. Hence, eq 4 allows us to formulate a sample-independent calibration procedure.

Since the exact functional forms of $g \equiv g(p_{ent})$, $l \equiv l(p_{ent})$, $t_0 \equiv t_0\left(\frac{p_{ent}}{K_0}\right)$ are not clearly known, we approximate them by a Taylor series according to

$$g(p_{ent}) = \sum_{n=1}^{\infty} g^{(n)} p_{ent}^n \tag{5a}$$

$$l(p_{ent}) = \sum_{r=1}^{\infty} l^{(r)} p_{ent}^r \tag{5b}$$

$$t_0\left(\frac{p_{ent}}{K_0}\right) = \sum_{s=0}^{\infty} t_0^{(s)}\left(\frac{p_{ent}}{K_0}\right)^s \tag{5c}$$

where superscripts n, r, and s denote the order of the expansion term (see section S1.6 of the Supporting Information for details). There are two benefits of approximating g, l, and t_0 by a Taylor series. First, a Taylor series provides a systematic approach to improve the calibration accuracy by adding higher order terms. Second, Taylor coefficients depend only weakly on the independent variable. Hence, $g^{(n)}$, $l^{(r)}$, $t_0^{(s)}$ can, to a good approximation, be considered independent of p_{ent} and K_0.

We insert eq 5a–5c into eq 4 to obtain our calibration function $E_m^{(n,r,s)}$ where n, r, and s are numbers corresponding to the highest orders included in the Taylor series for g, l, and t_0. (See eq S15 of the Supporting Information for more details.) Our calibration approach is thus based on a Taylor expansion of instrument properties (TEIP), and we use the nomenclature (n, r, s) to denote the calibration functions $E_m^{(n,r,s)}$.

For example, if we truncate g after second order, and l and t_0 after first order, we obtain the calibration function $E_m^{(2,1,1)}$

$$E_m^{(2,1,1)} = \frac{g^{(1)}p_{ent}}{K_0} + \frac{g^{(2)}p_{ent}^2}{K_0} - \sqrt{\frac{l^{(1)}p_{ent}}{K_0}}\theta - \left(t_0^{(0)} + t_0^{(1)}\frac{p_{ent}}{K_0}\right)\theta^2 \tag{6}$$

of our (2,1,1) TEIP model. Similarly, the calibration function $E_m^{(4,2,1)}$ of our (4,2,1) TEIP model is given by

DOI: 10.1021/acs.analchem.8b01326
Anal. Chem. 2018, 90, 9040−9047

$$E_m^{(4,2,1)} = \sum_{i=1}^{4} g^{(i)} \frac{p_{ent}^{i}}{K_0} - \theta \sqrt{\sum_{j=1}^{2} l^{(j)} \frac{p_{ent}^{j}}{K_0}} - \theta^2 \sum_{k=0}^{1} t_0^{(k)} \left(\frac{p_{ent}}{K_0} \right)^k \quad (7)$$

Calibration. We calibrate $g^{(1)}$, ..., $g^{(n)}$, $l^{(1)}$, ..., $l^{(r)}$, $t_0^{(0)}$, ..., $t_0^{(s)}$ by fitting $E_m^{(n,r,s)}$ to values of E_m measured for ESI tune mix ions for various p_{ent}, θ, E_0.

Evaluation. We use numerical root finding algorithms to determine the mobility K_0 of an unknown analyte from the measured value of E_m using the calibrated values of $g^{(1)}$, ..., $g^{(n)}$, $l^{(1)}$, ..., $l^{(r)}$, $t_0^{(0)}$, ..., $t_0^{(s)}$. Detailed steps including pseudo code and an example illustrating how to use the TEIP model to calibrate ion mobilities are given in sections S1.8 and S1.9 of the Supporting Information.

Accuracy. We evaluate the accuracy of our TEIP models by means of leave-k-out cross validation. Leave-k-out cross validation is an established method to evaluate how well a model will do when predicting for data it has not already seen during calibration. To this end, we divide the calibrant data set with n data points into a test set with k randomly chosen data points and a training set with $n - k$ data points. We determine the calibration coefficients from the training set and calculate the mean squared error in the model from the mobilities predicted for the test set. We perform leave-k-out cross validation with $k = 10$ on tune mix calibrant sets with $n = 340$ (TM1) and $n = 95$ (TM2) and repeat this process 5000 times to obtain distributions of the mean error for the TEIP calibration models.

The resulting error distributions (see Figure 3a and Table 2) show that our TEIP models reproduce drift tube mobilities to better than ~2% in 95% of the cases. The (4, 2, 1) models achieve 95th percentiles of ~0.8% and ~1.2% deviation from the drift tube values and perform better than the (2, 1, 1) models (95th percentiles of ~2%). The standard deviations suggest that the error distributions of the (4, 2, 1) models (σ = 0.1% and 0.2%) are slightly more narrow than those of the (2, 1, 1) models (σ = 0.3%). These observations underline that adding higher order Taylor expansion terms improves our calibration accuracy. Nevertheless, cross validation suggests that the (2, 1, 1) models reproduce drift tube values to better than 2−3%, which is comparable to the accuracy of drift tubes.[16] Detailed studies on structural isomers of small peptides, however, require an accuracy and precision of better than 2%[18,46] and, thus, higher order expansion terms in the calibration function. A systematic evaluation of how the accuracy of the TEIP models depends on (n, r, s) will be reported separately.

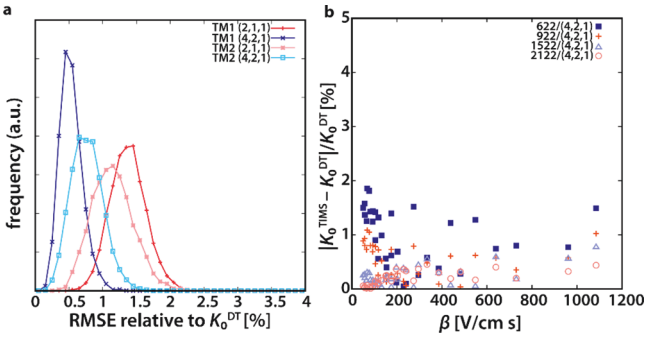

Figure 3. Accuracy of our TEIP models estimated by cross validation. (a) Distribution of the root-mean-squared error estimated by leave-10-out cross validation for different TEIP models ((2, 1, 1), (4, 2, 1)) and calibration sets (TM1, TM2). The 95th percentiles for the error distributions are below 2%. The (4, 2, 1) models are more accurate than the (2, 1, 1) models. (b) Correlation between the relative error and ramp rate β for the (4, 2, 1)/TM1 model. A trend is not apparent.

Table 2. Calibration Accuracy of our TEIP Method Estimated by Cross Validation[a,b]

	TM1		TM2	
model	(2, 1, 1)	(4, 2, 1)	(2, 1, 1)	(4, 2, 1)
mean error	1.3	0.5	1.1	0.7
standard deviation	0.3	0.1	0.3	0.2

[a]Drift tube values taken from Stow et al.[38] [b]Errors in percent deviation from the drift tube values calculated by leave-10-out cross validation.

Figure 3b correlates the error to the ramp rate β for the (4, 2, 1) model. The plot demonstrates that a systematic relationship between error and β does not exist. This observation contrasts with the currently used calibration procedures (Figure 2a), where the error increases systematically with β. The data thus indicate that our TEIP approach accurately determines ion mobilities for a variety of TIMS settings using a single set of calibration coefficients.

Small Peptide Systems. We focus on the protonated and sodiated pentapeptides SDGRG and GRGDS. These systems differ in ion mobility by less than 2%,[16,21] which allows us to estimate how well our approach performs in metabolomics or proteomics studies.

We recorded TIMS spectra for the two peptide systems under the same operating conditions (E_0 = 73.05 V/cm, p_{ent} = 2.00, 2.52, 2.80 mbar) as for Agilent tune mix (TM2). Details are found in Table S7. We calibrate mobilities for the SDGRG and GRGDS systems with our (2, 1, 1) and (4, 2, 1) TEIP models and correlate them to their drift tube values in Figure 4a. The data show that all calibrated mobilities fall within ±2% of the drift tube mobilities. This observation is important because it means that our calibration models reproduce the drift tube mobilities within their reported margin of error of 2−3%.[16] More specifically, Table 1 and Figure 4b reveal that ion mobilities calibrated by the (2, 1, 1) and (4, 2, 1) TEIP models for these peptide systems deviate from their drift tube values on average by 0.8% and 0.5%. The 95th percentiles are 1.7% and 1.0%, respectively. These values are consistent with, and thus support, the cross-validation analysis discussed in the previous section.

Figure 4c shows distributions of cross sections calibrated according to our (4, 2, 1) scheme for the four peptide systems under various experimental settings. The plot depicts narrow, well-separated distributions for SDGRG and GRGDS. This highlights that our (4, 2, 1) model accurately predicts ion mobilities for various entrance pressures and ramp rates.

Transferability. We assess transferability of our TEIP approach over time, toward different TIMS settings as well as to compound classes and charge states distinct from those of the calibrants. To this end, we calibrate TIMS data recorded over a time span of approximately 11 months for different compound classes (TAA, TM, SDGRG/GRGDS) and various experimental settings (p_{ent}, β, E_0). Tune mix calibrant data were recorded at the beginning (TM1) and at the end (TM2) of this 11-month period. We calibrate our (2, 1, 1) and (4, 2, 1) models by both sets of tune mix data and correlate the

DOI: 10.1021/acs.analchem.8b01326
Anal. Chem. 2018, 90, 9040−9047

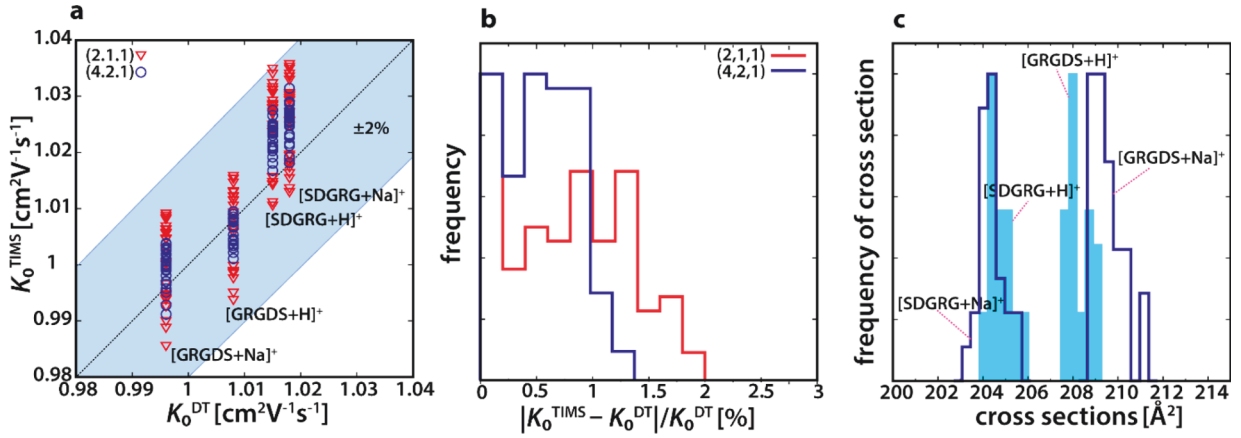

Figure 4. Accuracy of our TEIP models for the protonated and sodiated pentapeptides SDGRG and GRGDS for various TIMS settings. (a) Correlation between calibrated mobilities and drift tube mobilities. (b) Error distribution of calibrated mobilities K_0^{TIMS} using the (2, 1, 1) and (4, 2, 1) models. All calibrated mobilities fall within the ±2−3% margin of error reported for the drift tube mobilities. (c) Reproducibility of cross sections calibrated by the (4, 2, 1) model for various TIMS settings. The SDGRG and GRGDS systems are well separated. The reference cross sections measured on a drift tube were taken from ref 16 ([SDGRG + Na]$^+$:203.5 Å^2, [SDGRG + H]$^+$:204.6 Å^2, [GRGDS + H]$^+$:205.9 Å^2, [GRGDS + Na]$^+$:208.2 Å^2).

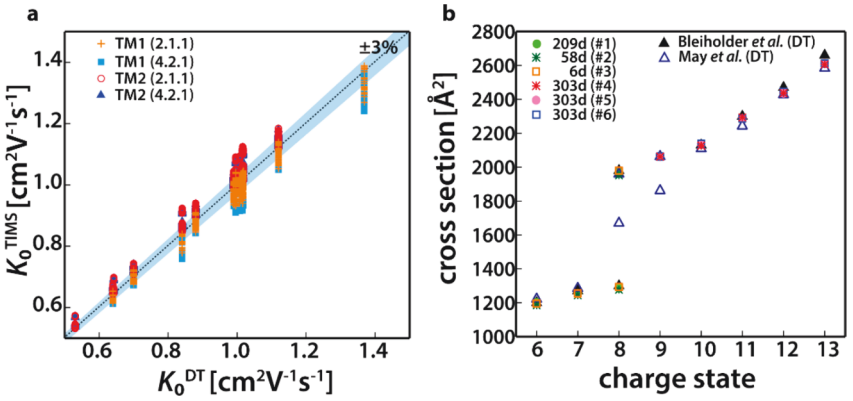

Figure 5. Transferability of our TEIP models. (a) Correlation between calibrated ion mobilities and their drift tube values for various samples (tune mix, TAA, SDGRG/GRGDS). Measurements were conducted over ∼11 months with calibration performed at the beginning (TM1) and the end (TM2). The plot includes over 4500 data points. (b) Cross sections of ubiquitin plotted as a function of their charge state (+6 to +13). The figure compares drift tube cross sections to cross sections calibrated with our (2, 1, 1)/TM2 model from TIMS spectra with up to ∼300 days delay between calibration and measurement. Drift tube values are taken from refs 35 and 47 with a reported error of 2−3%.

calibrated ion mobilities to their drift tube values[16,35,38] in Figure 5a. The figure depicts more than 4500 data points (see Tables S7−S12 for details). Note that this is the "worst-case" scenario for calibration, because calibration would typically occur on a daily or weekly basis. Nevertheless, linear regression analysis (Table S13) yields slopes ranging from 0.980 to 1.036. This indicates that the calibrated mobilities correlate strongly with the drift tube mobilities. We assess the quality of the correlation by means of an F-test (Table S13). The p-values of the F-tests are less than 0.001 for all calibration models. This means that we have >99.9% confidence that the calibrated ion mobilities are linearly correlated to the drift tube values.

We recorded TIMS spectra for ubiquitin under different solvent conditions and different settings of β or E_0 over a period of 11 months (see Table S14 for details). We calibrate mobilities for charge states +6 to +13 by our (2, 1, 1) model with TM2 and compare the calibrated cross sections to those measured on drift tubes[35,47] in Figure 5b. The equivalent plot is shown in Figure S4 for calibration with TM1. The plots show that TIMS and drift tube cross sections agree to within ∼0.2−2%, irrespective of the calibrant data used. Note that the delay between calibration and measurement ranges from approximately 3 to 303 days. Thus, the data provide further evidence that our calibration scheme is robust for transfer over time as well as to compound classes and charge states not included in the calibrant data.

For clarity and brevity, a systematic analysis of how strongly the calibration accuracy decays with delay between calibration and measurements will follow separately.

SUMMARY AND CONCLUSIONS

We assessed the accuracy and limitations of the currently used calibration procedure in TIMS. Our data show that high ramp rates in the TIMS analyzer can introduce calibration errors on the order of a few percent. For the typically used ramp rates, however, the currently used calibration models are found to reproduce drift tube mobilities to ∼1% (95th percentile).

Further, we developed a transferable and sample-independent calibration procedure for TIMS. The central aspects of our approach are (1) a calibration function that is derived from a solution to the Boltzmann transport equation and (2) calibration coefficients that are, to a good approximation,

DOI: 10.1021/acs.analchem.8b01326
Anal. Chem. 2018, 90, 9040−9047

constant and independent of instrument settings or sample properties. These calibration constants are based on a Taylor expansion of instrument properties (TEIP). Our analysis reveals that our TEIP approach is sufficiently accurate (95th percentile approximately 1−2%) to characterize structural isomers of small compounds as well as conformations of protein ions.

■ ASSOCIATED CONTENT

Supporting Information

The Supporting Information is available free of charge on the ACS Publications Web site. The Supporting Information is available free of charge on the ACS Publications website at DOI: 10.1021/acs.analchem.8b01326.

Mobilities for Agilent ESI tune mix; list of terms and variables; derivation of TEIP models developed in this work; example and pseudo code demonstrating how to use the TEIP models; detailed description of materials, sample preparation, TIMS methods; calibration constants obtained using the currently used calibration scheme; calibrated mobilities for various molecular systems; cross validation method estimating prediction precision and accuracy
(PDF)

■ AUTHOR INFORMATION

Corresponding Author

*E-mail: cbleiholder@fsu.edu.

ORCID

Mengqi Chai: 0000-0002-6363-0216

Author Contributions

The manuscript was written through contributions of all authors.

Notes

The authors declare no competing financial interest.

■ ACKNOWLEDGMENTS

This work was supported by the National Science Foundation under grant CHE-1654608. The authors thank M. E. Ridgeway and M. A. Park for commenting on the manuscript and helpful discussions.

■ REFERENCES

(1) Revercomb, H. E.; Mason, E. A. *Anal. Chem.* **1975**, *47*, 970−983.
(2) Mason, E. A.; McDaniel, E. W. *Transport Properties of Ions in Gases*; Wiley-VCH: Weinheim, Germany, 1988.
(3) Kanu, A. B.; Dwivedi, P.; Tam, M.; Matz, L.; Hill, H. H. *J. Mass Spectrom.* **2008**, *43*, 1−22.
(4) Lanucara, F.; Holman, S. W.; Gray, C. J.; Eyers, C. E. *Nat. Chem.* **2014**, *6*, 281−294.
(5) Bleiholder, C.; Bowers, M. T. *Annu. Rev. Anal. Chem.* **2017**, *10*, 365−386.
(6) Jurneczko, E.; Barran, P. E. *Analyst* **2011**, *136*, 20−28.
(7) Bernstein, S. L.; Dupuis, N. F.; Lazo, N. D.; Wyttenbach, T.; Condron, M. M.; Bitan, G.; Teplow, D. B.; Shea, J.-E.; Ruotolo, B. T.; Robinson, C. V.; Bowers, M. T. *Nat. Chem.* **2009**, *1*, 326−331.
(8) Bleiholder, C.; Dupuis, N. F.; Wyttenbach, T.; Bowers, M. T. *Nat. Chem.* **2011**, *3*, 172−177.
(9) Bleiholder, C.; Do, T. D.; Wu, C.; Economou, N. J.; Bernstein, S. S.; Buratto, S. K.; Shea, J.-E.; Bowers, M. T. *J. Am. Chem. Soc.* **2013**, *135*, 16926−16937.
(10) Uetrecht, C.; Barbu, I. M.; Shoemaker, G. K.; van Duijn, E.; Heck, A. J. R. *Nat. Chem.* **2011**, *3*, 126−132.
(11) Ruotolo, B. T.; Benesch, J. L. P.; Sandercock, A. M.; Hyung, S.-J.; Robinson, C. V. *Nat. Protoc.* **2008**, *3*, 1139−1152.
(12) Bornschein, R. E.; Ruotolo, B. T. *Analyst* **2015**, *140*, 7020−7029.
(13) Quintyn, R. S.; Harvey, S. R.; Wysocki, V. H. *Analyst* **2015**, *140*, 7012−7019.
(14) Fenn, L. S.; Kliman, M.; Mahsut, A.; Zhao, S. R.; McLean, J. A. *Anal. Bioanal. Chem.* **2009**, *394*, 235−244.
(15) Hines, K. M.; May, J. C.; McLean, J. A.; Xu, L. *Anal. Chem.* **2016**, *88*, 7329−7336.
(16) May, J. C.; Goodwin, C. R.; Lareau, N. M.; Leaptrot, K. L.; Morris, C. B.; Kurulugama, R. T.; Mordehai, A.; Klein, C.; Barry, W.; Darland, E.; Overney, G.; Imatani, K.; Stafford, G. C.; Fjeldsted, J. C.; McLean, J. A. *Anal. Chem.* **2014**, *86*, 2107−2116.
(17) Jeanne Dit Fouque, K.; Garabedian, A.; Porter, J.; Baird, M.; Pang, X.; Williams, T. D.; Li, L.; Shvartsburg, A.; Fernandez-Lima, F. *Anal. Chem.* **2017**, *89*, 11787−11794.
(18) Dodds, J. N.; May, J. C.; McLean, J. A. *Anal. Chem.* **2017**, *89*, 952−959.
(19) Meier, F.; Beck, S.; Grassl, N.; Lubeck, M.; Park, M. A.; Raether, O.; Mann, M. *J. Proteome Res.* **2015**, *14*, 5378−5387.
(20) Bleiholder, C. *Int. J. Mass Spectrom.* **2016**, *399*−*400*, 1−9.
(21) Kemper, P. R.; Dupuis, N. F.; Bowers, M. T. *Int. J. Mass Spectrom.* **2009**, *287*, 46−57.
(22) Wyttenbach, T.; Kemper, P. R.; Bowers, M. T. *Int. J. Mass Spectrom.* **2001**, *212*, 13−23.
(23) Ujma, J.; Giles, K.; Morris, M.; Barran, P. E. *Anal. Chem.* **2016**, *88*, 9469−9478.
(24) Pringle, S. D.; Giles, K.; Wildgoose, J. L.; Williams, J. P.; Slade, S. E.; Thalassinos, K.; Bateman, R. H.; Bowers, M. T.; Scrivens, J. H. *Int. J. Mass Spectrom.* **2007**, *261*, 1−12.
(25) Fernandez-Lima, F.; Kaplan, D. A.; Suetering, J.; Park, M. A. *Int. J. Ion Mobility Spectrom.* **2011**, *14*, 93−98.
(26) Michelmann, K.; Silveira, J. A.; Ridgeway, M. E.; Park, M. A. *J. Am. Soc. Mass Spectrom.* **2015**, *26*, 14−24.
(27) Silveira, J. A.; Michelmann, K.; Ridgeway, M. E.; Park, M. A. *J. Am. Soc. Mass Spectrom.* **2016**, *27*, 585−595.
(28) Deng, L.; Webb, I. K.; Garimella, S. V. B.; Hamid, A. M.; Zheng, X.; Norheim, R. V.; Prost, S. A.; Anderson, G. A.; Sandoval, J. A.; Baker, E. S.; Ibrahim, Y. M.; Smith, R. D. *Anal. Chem.* **2017**, *89*, 4628−4634.
(29) Bush, M. F.; Hall, Z.; Giles, K.; Hoyes, J.; Robinson, C. V.; Ruotolo, B. T. *Anal. Chem.* **2010**, *82*, 9557−9565.
(30) Hernandez, D. R.; DeBord, J. D.; Ridgeway, M. E.; Kaplan, D. A.; Park, M. A.; Fernandez-Lima, F. *Analyst* **2014**, *139*, 1913−1921.
(31) Silveira, J. A.; Ridgeway, M. E.; Park, M. A. *Anal. Chem.* **2014**, *86*, 5624−5627.
(32) Liu, F. C.; Kirk, S. R.; Bleiholder, C. *Analyst* **2016**, *141*, 3722−3730.
(33) Molano-Arevalo, J. C.; Jeanne Dit Fouque, K.; Pham, K.; Miksovska, J.; Ridgeway, M. E.; Park, M. A.; Fernandez-Lima, F. *Anal. Chem.* **2017**, *89*, 8757−8765.
(34) Liu, F. C.; Ridgeway, M. E.; Park, M. A.; Bleiholder, C. *Analyst* **2018**, *143*, 2249−2258.
(35) Bleiholder, C.; Johnson, N. R.; Contreras, S.; Wyttenbach, T.; Bowers, M. T. *Anal. Chem.* **2015**, *87*, 7196−7203.
(36) Haler, J. R. N.; Kune, C.; Massonnet, P.; Comby-Zerbino, C.; Jordens, J.; Honing, M.; Mengerink, Y.; Far, J.; De Pauw, E. *Anal. Chem.* **2017**, *89*, 12076−12086.
(37) Schenk, E. R.; Almeida, R.; Miksovska, J.; Ridgeway, M. E.; Park, M. A.; Fernandez-Lima, F. *J. Am. Soc. Mass Spectrom.* **2015**, *26*, 555−563.
(38) Stow, S. M.; Causon, T. J.; Zheng, X.; Kurulugama, R. T.; Mairinger, T.; May, J. C.; Rennie, E. E.; Baker, E. S.; Smith, R. D.; McLean, J. A.; Hann, S.; Fjeldsted, J. C. *Anal. Chem.* **2017**, *89*, 9048−9055.
(39) Wyttenbach, T.; von Helden, G.; Batka, J. J.; Carlat, D.; Bowers, M. T. *J. Am. Soc. Mass Spectrom.* **1997**, *8*, 275−282.

DOI: 10.1021/acs.analchem.8b01326
Anal. Chem. 2018, 90, 9040−9047

(40) von Helden, G.; Wyttenbach, T.; Bowers, M. T. *Int. J. Mass Spectrom. Ion Processes* **1995**, *146*, 349−364.
(41) Wyttenbach, T.; Pierson, N. A.; Clemmer, D. E.; Bowers, M. T. *Annu. Rev. Phys. Chem.* **2014**, *65*, 175−196.
(42) Siems, W. F.; Viehland, L. A.; Hill, H. H. *Analyst* **2016**, *141*, 6396−6407.
(43) Morsa, D.; Gabelica, V.; De Pauw, E. *Anal. Chem.* **2011**, *83*, 5775−5782.
(44) Morsa, D.; Gabelica, V.; De Pauw, E. *J. Am. Soc. Mass Spectrom.* **2014**, *25*, 1384−1393.
(45) Benigni, P.; Porter, J.; Ridgeway, M. E.; Park, M. A.; Fernandez-Lima, F. *Anal. Chem.* **2018**, *90*, 2446−2450.
(46) Fasciotti, M.; Sanvido, G. B.; Santos, V. G.; Lalli, P. M.; McCullagh, M.; de Sá, G. F.; Daroda, R. J.; Peter, M. G.; Eberlin, M. N. *J. Mass Spectrom.* **2012**, *47*, 1643−1647.
(47) May, J. C.; Jurneczko, E.; Stow, S. M.; Kratochvil, I.; Kalkhof, S.; McLean, J. A. *Int. J. Mass Spectrom.* **2018**, *427*, 79−90.

DOI: 10.1021/acs.analchem.8b01326
Anal. Chem. 2018, 90, 9040−9047